Gaussian Scale-space Dense Disparity Estimation with Anisotropic Disparity-field Diffusion

Jangheon Kim and Thomas Sikora
Department of Communication Systems, Technical University of Berlin
Einsteinufer 17, Berlin, Germany
E-mail : {j.kim, sikora}@nue.tu-berlin.de

Abstract

We present a new reliable dense disparity estimation algorithm which employs Gaussian scale-space with anisotropic disparity-field diffusion. This algorithm estimates edge-preserving dense disparity vectors using a diffusive method on iteratively Gaussian-filtered images with a scale, i.e. the Gaussian scale-space.

While a Gaussian filter kernel generates a coarser resolution from stereo image pairs, only strong and meaningful boundaries are adaptively selected on the resolution of the filtered images. Then, coarse global disparity vectors are initialized using the boundary constraint. The per-pixel disparity vectors are iteratively obtained by the local adjustment of the global disparity vectors using an energy-minimization framework. The proposed algorithm preserves the boundaries while inner regions are smoothed using anisotropic disparity-field diffusion.

In this work, the Gaussian scale-space efficiently avoids illegal matching on a large baseline by the restriction of the range. Moreover, it prevents the computation from iterating into local minima of ill-posed diffusion on large gradient areas e.g. shadow and texture region, etc. The experimental results prove the excellent localization performance preserving the disparity discontinuity of each object.

1. Introduction

As three-dimensional imaging systems are becoming increasingly popular, depth estimation has developed into a key research area. Many disparity estimation algorithms which intended to solve the correspondence problem for depth estimation have been developed over the last 30 years. For example, feature-based methods [1, 2] extract features such as corners, lines, curves or edges from image pairs and then establish correspondences between them. Their main advantage is the small amount of data required based on the accurate information, drawback is the insufficient information available to generate accurate depth. Area-based methods [3, 4, 5] can provide more reliable estimation performance by correlating image patches in relatively textured areas. Research trends to concentrate on hybrid area-based approaches which combine the above two approaches for good localization performance. The hybrid area-based approaches use some constraints between features [6], multiple-windows [7, 8, 9], global disparity constraints [10], among others. However, performance is not satisfactory for producing a dense field with full resolution because of inherent localization problems due to noise, occlusions, textures, etc.

In this paper, we improve the performance of hybrid system. To this end we employ multiple-resolutions and their scales to provide the best trade-off between the detected features and the localization performance. Latest research using multiple resolutions focuses on energy-based approaches that iteratively minimize an energy function with a regularization formulation [11, 12, 13, 14, 15, 16]. This approach achieves high-accurate results smoothing homogeneous areas and preserving strong features. However, local minima and computational cost to solve PDEs (partial differential equations) are very high.

Recent energy-based approaches employ anisotropic diffusion as the regularization term to prevent important edges from over-smoothing. Anisotropic diffusion methods were proposed to accomplish image restoration and enhancement by Perona and Malik [17]. The basic idea is to modify the diffusion coefficient at edges with steep intensity gradients. The method has been applied for disparity estimation and depth estimation. The method shows smoothed but detailed results in some images [12, 14, 15]. Unfortunately, the Perona and Malik model is still ill-posed because of true backward diffusion in areas of large gradients. The model usually yields unexpected wrong directional diffusions on homogeneous texture areas. Catt´e *et al*. [18] solved the problem for image

Proceedings of the Fifth International Conference on 3-D Digital Imaging and Modeling (3DIM'05)
1550-6185/05 $20.00 © 2005 **IEEE**

enhancement by considering the gradient evaluation on the pre-filtered image by a Gaussian-filter kernel instead of exact intensity gradient. This method recently turned out to be well-posed and edges are still enhanced [19]. The evolution using a Gaussian pre-filtering avoids the detection and the emphasis of initial noise. We propose a novel algorithm to solve the correspondence problem for stereo image pairs. The proposed algorithm implements a progressive combination of two mentioned complementary contributions between the hybrid area-based approach and the energy-based approach. The solution is iteratively calculated on the multiple resolutions of a Gaussian scale-space.

In a first step, Gaussian scale-space is iteratively generated to a coarser resolution by convolving a stereo image pair with the Gaussian-filter kernel. Only strong and meaningful boundaries are probability-adaptively determined on the resolution of the filtered image. Next, coarse but trustworthy disparity vectors are initialized as global disparity ranges using a boundary constraint. Dense disparity vectors are obtained by iterative adjustment into a fine resolution using energy minimization procedure with anisotropic disparity-field diffusion.

In the follow section, we describe the algorithm in detail using two steps: Gaussian scale-space disparity initialization and dense disparity estimation with anisotropic disparity-field diffusion

2. Gaussian scale-space dense disparity estimation with anisotropic disparity-field diffusion

2.1. Gaussian scale-space disparity initialization

The scale-space theory is based on a lot of research for edge detection. For example, Canny [20] proposed a successful edge detector which uses the approximation by the first derivative of a Gaussian. By convolving an image with single Gaussian-filter, the edges are detected very precisely at the maximum of the gradient magnitude in the Gaussian-smoothed image. Witkin [21] developed the Canny edge detector into an iterative method for multi-resolution processes, i.e. Gaussian scale-spaces. A coarser resolution image is iteratively generated by convolving the image with a Gaussian-filter kernel. The scale parameter of Gaussian-filter kernel is used to control the boundary strength and direction to be detected. This parameter tuning results in strong boundaries only, which have larger values than can be detected in the specified scale [24].

Figure 1-(a) illustrates Gaussian scale-space using one-dimension (i.e. a horizontal line) and its boundary is shown in Figure 1-(b). The boundary should be obtained at the position of discontinuity for the best localization performance. Thus, we estimate the position using partial differential as follows:

First, we obtain the scale-space using standard deviation of the Gaussian. A two-dimensional Gaussian-filter kernel is defined as

$$\begin{aligned} \mathcal{G}_\sigma(x,y) &= \mathcal{G}_\sigma * I(x,y) \\ &= (2\pi\sigma^2)^{-1} e^{-(x^2+y^2)/(2\sigma^2)} * I(x,y) \end{aligned} \quad (1)$$

where $\mathcal{G}_\sigma(x,y)$ is the image intensity filtered by local convolution kernel of the Gaussian $\mathcal{G}_\sigma$ at a scale-level σ. The first derivative of Gaussian along the x-axis is given in Eq. (2) and the other along y-axis is obtained in a similar way.

$$\nabla_x \mathcal{G}_\sigma = \frac{\partial \mathcal{G}_\sigma}{\partial x} = \frac{-x}{\sqrt{2\pi\sigma^3}} e^{-x^2/2\sigma^2} = -\frac{x}{\sigma^2}\mathcal{G}_\sigma \quad (2)$$

Since the two-dimensional gradient is a first-order operator $(\partial/\partial x, \partial/\partial y)$ defined as a vector, the direction of the gradient is defined by the Euclidean norm of gradient which consequently indicates the strength of the intensity change as

$$\begin{aligned} \left|\nabla \mathcal{G}_\sigma(x,y)\right| &= \left| I(x,y) * \frac{\partial}{\partial N}\mathcal{G}_\sigma(x,y) \right| \\ &= \sqrt{\left(\frac{\partial \mathcal{G}_\sigma(x,y)}{\partial x}\right)^2 + \left(\frac{\partial \mathcal{G}_\sigma(x,y)}{\partial y}\right)^2} \end{aligned} \quad (3)$$

(a) Gaussian scale-space (a horizontal line)

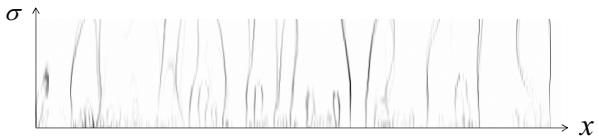

(b) boundary of the Gaussian scale-space

Figure 1. Gaussian scale-space

In Eq. (3), N represents a unit vector towards an arbitrary gradient direction. The gradient direction is perpendicular to the edge orientation and localizes the boundary. Thus, the equivalent function considering several directional derivatives can be easily expressed with respect to a polar coordinate system where $r(\theta)=\sqrt{x^2+y^2}$ represents the radial distance from the origin. The function is symmetrical and independent of the orientation θ. The prediction error is defined as

$$E_\zeta[\mathcal{G}_\sigma(r),\theta]=\left|\mathcal{G}_\sigma(x+d\cos\theta,y+d\sin\theta)-\mathcal{G}_\sigma(x,y)\right| \quad (4)$$

where ζ is the boundary domain and d is the distance of the prediction, which is proportional to the scale. If we consider two possible directions for the morphology of a boundary, forward is θ and backward is given as $(\theta+\pi)$. The probability P is assigned in a proportion to their prediction errors [25] in Eq. (5).

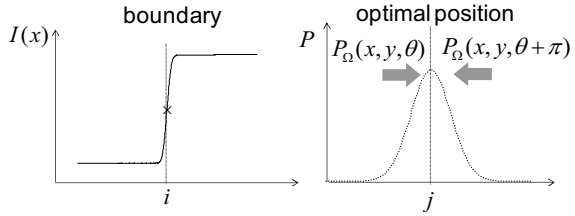

(a) boundary position on a scale-space i (b) local maxima of intensity changes j

Figure 2. Boundary of Gaussian scale-space

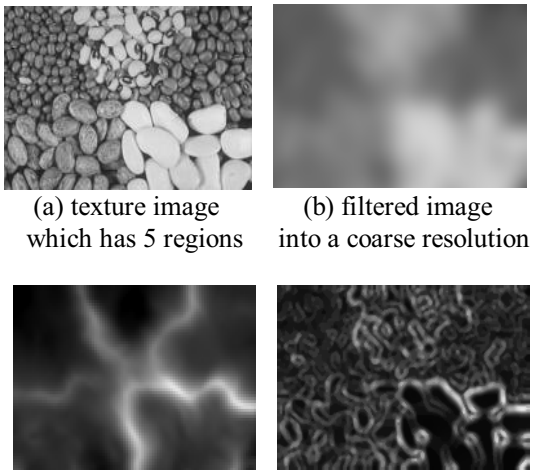

(a) texture image which has 5 regions (b) filtered image into a coarse resolution

(c) boundary image of a coarse resolution (d) boundary image of a fine resolution

Figure 3. Morphological course-to-fine hierarchy of a texture image

$$P_\zeta[\mathcal{G}_\sigma(r),\theta]=\frac{E_\zeta[\mathcal{G}_\sigma(r),\theta]}{E_\zeta[\mathcal{G}_\sigma(r),\theta]+E_\zeta[\mathcal{G}_\sigma(r),(\theta+\pi)]} \quad (5)$$

A large prediction error in a certain direction implies higher possibility to identify local maxima of intensity changes by analyzing the total certainties over half circles as

$$\arg\max_\theta \int_{\theta-\pi/2}^{\theta+\pi/2} P_\zeta[\mathcal{G}_\sigma(r),\theta]d\theta \quad (6)$$

Figure 2 illustrates the method to detect the boundary of Gaussian scale-space. In Figure 2-(a), the optimal position of a boundary i of a scale is estimated to minimize errors by the highest possibility, thus i is located at the maxima of intensity changes j. Since the maximum of change directly implies the position of discontinuity, i is exactly located at the position of discontinuity on the scale as Figure 2-(b) illustrates.

The smoothness condition of Gaussian scale-space can be efficiently used to accommodate an object with several piecewise smooth edges, i.e. a texture object. On a coarse resolution, the piecewise edges can be smoothly removed and an object is determined as an arbitrarily shaped region of a coarse resolution. Therefore, Gaussian scale-space represents a coarse-to-fine morphological hierarchy of ROI (region of interest) which has the shape trajectory of discontinuity. Figure 3 exemplifies the morphological course-to-fine hierarchy.

In the shape trajectory, coarse but trustworthy dense disparity vectors are iteratively estimated using the concept of a hybrid area-based approach which was described in Section 1. Subsequently, the coarse disparity vector field is iteratively updated into a fine disparity vector field. Iterating into local minima can be efficiently avoided using this method. A hybrid area-based approach which uses both edges and regions is implemented with a matching energy function which uses a squared difference. For illustration purpose, the energy function will be separately formulated with two energy functions which are respectively laid on the boundary domain ξ and region domain Ω.

In a first step, trustworthy global disparity vectors on the boundary domain ξ are horizontally and vertically estimated following the pixels at boundary position as

$$E_\zeta(\tilde{\mathrm{D}})=\int_\zeta\left[I_l(x,y)-I_r\left(x+\tilde{\mathrm{D}}_{l\to r}(x,y),y\right)\right]^2 dxdy \quad (7)$$

$\tilde{\mathrm{D}}_{l\to r}(x,y)$ is the range of global disparity vectors and

the subscripts denote the matching direction, e.g. $l \to r$ for left-to-right direction.

When a region enclosed in the boundary is initialized with the range of the global disparity vectors using the boundary constraint, dense disparity vectors are locally and iteratively estimated by the detail adjustment. This method offers a more accurate local disparity estimation solution to restrict error. Moreover, it can be used to smooth a homogeneous region in a disparity field. We note that a homogeneous region generally has similar disparities because the physical world is cohesive. The adjustment is described as an error minimization procedure, which is coupled with anisotropic disparity-field diffusion in the next section.

2.2. Dense disparity estimation with anisotropic disparity-field diffusion

Although the minimization of matching errors is a common solution in the stereo correspondence problem, it does not always guarantee the homogeneous proposition. Traditional solutions frequently consider an additional smoothing term for regularization. However, smoothing over disparity boundaries often causes conspicuous blurring errors.

In this paper, we regularize a disparity vector field by an edge-preserving anisotropic diffusion term. As we will show, this yields excellent results without smoothing the important boundaries. We propose to adjust the disparity vector field via PDE in an energy-minimization framework with a regularization term as

$$E_{\Omega}(d) = \int_{\Omega}[I_l(x,y) - I_r(x + d_{l\to r}(x) \in \tilde{\mathrm{D}}(x,y), y)]^2 dxdy + \lambda \int_{\Omega} \psi[\nabla \mathcal{G}_{l,\sigma}(x,y), \nabla d_{l\to r}(x,y)]dxdy \quad (8)$$

where Ω is the region domain and $\tilde{\mathrm{D}}$ is the constraint of a global disparity range on the boundary domain ξ in Eq. (7) . Dense disparity vectors $d_{l\to r}$ are estimated in the global disparity range $\tilde{\mathrm{D}}$. λ is a Lagrange multiplier and $\psi(\nabla)$ is a modified version for disparity of the discrete Perona and Malik model [26], which has a form as $G(\nabla)\nabla'$ in the flux function as

$$\psi[\nabla \mathcal{G}_{l,\sigma}(x,y), \nabla d_{l\to r}(x,y)]dxdy = G(\left\|\nabla \mathcal{G}_{l,\sigma}\right\|)\nabla d_{l\to r} \quad (9)$$

$G(\nabla)$ is an anisotropic diffusion function which (is called "*edge-stopping function*") – used to modify the diffusion coefficient at edges and to derive discontinuity. A suitable choice of G is

$$G(s) = e^{-(\nabla^2/K^2)} \quad (10)$$

for a positive constant K that controls the level of contrast of edges to affect the smoothing process. Figure 4 depicts the anisotropic diffusion functions $\psi(\nabla)$ and $G(\nabla)$. The value of each function is reduced when the absolute value of the gradient magnitude increases beyond a fixed point determined by the scale parameter. This modified flux function $\psi(\nabla) = G(\nabla)\nabla'$ calculates the divergence between the gradient of disparity field and the gradient of filtered image. This function suppresses the diffusion at the important discontinuity boundary which has large gradients for both the disparity field (e.g. left-to-right disparity) and the Gaussian filtered base-image (e.g. left image). As mentioned in section 1, anisotropic diffusion methods employing Gaussian-filter kernels solve the ill-posed true backward diffusion in areas of large gradients, e.g. shadow and texture region, etc. [18, 19]. Similarly, disparity field diffusion depends on the image gradient. Thus, a large image gradient on a homogeneous area converges into the local minima. The proposed method solves the local minima problem by the gradient evaluation based on the Gaussian pre-filtered base-image. The left-to-right disparity field is diffusively regularized by evaluation of the gradient based on the Gaussian filtered base-image of Eq. (11). The right-to-left disparity field is vice-versa.

$$\mathcal{G}_{l,\sigma}(x,y) = \mathcal{G}_{\sigma} * I_l(x,y) = (2\pi\sigma^2)^{-1} e^{-(x_l^2 + y_l^2)/(2\sigma^2)} * I_l(x,y) \quad (11)$$

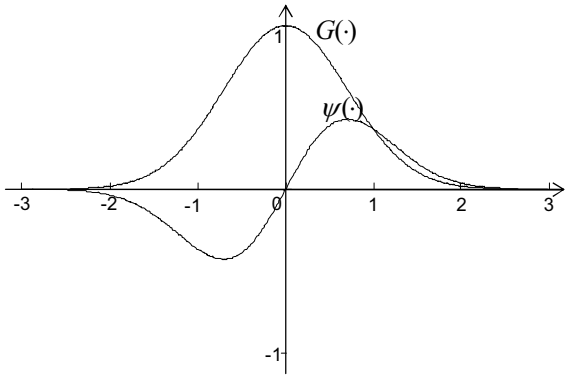

Figure 4. Anisotropic diffusion function

As shown in section 2.1, a shape trajectory with a local region is determined towards it's closest image boundaries to minimize prediction errors. The disparity vector field inside the local region is diffusively regularized to all its neighbors toward the propagation direction. Diffusion is a process that equilibrates spatial variations with concentration. We iteratively solve the minimization problem of Eq. (8) using the Euler-Langrange equation and the asymptotic analysis of the parabolic PDE [11, 12, 13] with natural boundary conditions in Eq. (12).

$$\partial_t d_{l\to r}(x,y,t) = \lambda \mathrm{div}\left[\mathrm{G}\left(\left\| \nabla \mathcal{G}_{l,\sigma}(x,y) \right\| \right) \nabla d_{l\to r}(x,y) \right] \quad (12)$$
$$+ \frac{\partial I_r(x + d_{l\to r}(x), y)}{\partial x} \left[I_l(x,y) - I_r(x + d_{l\to r}(x), y) \in \tilde{\mathrm{D}}_{l\to r}(x,y) \right]$$

When a scale of successively smoothed, the features are obtained from Eq. (9), the solution of this parabolic problem coincides with the filtering of the initial disparity field in Eq. (12). Since we have described the regularization term using nonlinear PDE on a disparity field, the next step is to discretize the parabolic equation of the PDE in space and time by finite differences. In this paper, an inhomogeneous time diffusion process with discrete sampling solves the problem as

$$\frac{d^{t+1}_{l\to r} - d^{t}_{l\to r}}{\tau_x} = \lambda \mathrm{div}\left[\mathrm{G}\left(\left\| \nabla \mathcal{G}_{l,\sigma}(x,y) \right\| \right) \nabla d^{t}_{l\to r}(x,y) \right] + \quad (13)$$
$$\frac{\partial I_r(x + d^{t}_{l\to r}(x), y)}{\partial x} \left[\left[I_l(x,y) - I_r(x + d_{l\to r}(x), y) \in \tilde{\mathrm{D}}_{l\to r}(x,y) \right] \right.$$
$$\left. + \frac{\partial I_r(x + d^{t}_{l\to r}(x), y)}{\partial x} (d^{t+1}_{l\to r} - d^{t}_{l\to r}) \right]$$

In the inhomogeneous time diffusion of Eq. (13), different pixels diffuse at a different time scale related to the pixel confidence. High confidence pixels diffuse much slower than low confidence pixels [11]. To increase the time step τ_x on the scale-space, the disparity field is successfully smoothed and coarsened. Simultaneously, boundaries are enhanced if one chooses a nonlinear edge-stopping function $G(\nabla)$ which suppresses diffusion in area of high gradients from scale-space. A lot of spatially varying diffusion functions to control the rate at which diffusion occurs near the edges have been proposed and evaluated [27]. Eq. (10) achieved sufficient and reliable results for our purpose.

The regularization term includes two steps: the gradient and the divergence. Numerically, we do not use central difference approximation for the gradient and the divergence, because this would result in an unconditionally unstable scheme. We instead employ forward differences for gradient and backward differences for the divergence in Eq. (14) and (15).

$$\frac{\partial I(x,y)}{\partial x} \approx \delta_x^{(+)} I(x,y), \frac{\partial I(x,y)}{\partial y} \approx \delta_y^{(+)} I(x,y) \quad (14)$$

$$div\left[\mathrm{G}(\nabla)\nabla' \right] \approx \delta_x^{(-)} \left[\mathrm{G}(\nabla)\nabla' \right] + \delta_y^{(-)} \left[\mathrm{G}(\nabla)\nabla' \right] \quad (15)$$

$(+)$ and $(-)$ respectively denote the forward direction and the backward direction of the gradient operator. In the two dimensional case, the gradient operator yield a 2×2 matrix, and the divergence operator collapses this into a 2×1 vector. While the edge stopping function $G(\nabla)$ is calculated, the nonlinear disparity diffusion requires the computation of flux function $\psi(\nabla) = G(\nabla)\nabla'$ in x and y directions. The columns of the flux matrix are computed independently and the backward differences of the flux matrix are used to compute the divergence operation. Finally we obtain the numerical form of Eq. (13) in Eq (16).

$$\frac{d^{t+1}_{l\to r} - d^{t}_{l\to r}}{\tau_x} = \lambda \left[\delta_x^{(-)} \left(e^{-\left[\delta_x^{(+)}\left(\mathcal{G}_{l,\sigma}(x,y)\right)^2 / K^2\right]} \delta_x^{(+)} d^{t}_{l\to r}(x,y) \right) \right.$$
$$\left. + \delta_y^{(-)} \left(e^{-\left[\delta_y^{(+)}\left(\mathcal{G}_{l,\sigma}(x,y)\right)^2 / K^2\right]} \delta_y^{(+)} d^{t}_{l\to r}(x,y) \right) \right] \quad (16)$$
$$+ \delta_x^{(+)} d_{l\to r}(x) \left[\left(I_l(x,y) - I_r(x + d^{t}_{l\to r}(x), y) \in \tilde{\mathrm{D}}_{l\to r}(x,y) \right) \right.$$
$$\left. + \delta_x^{(+)} I_r(x,y)(d^{t+1}_{l\to r} - d^{t}_{l\to r}) \right]$$

3. Simulation results

3.1. Performance under natural image conditions

Future 3D object-based vision systems for multimedia and tele-immersion should be robust for indoor and outdoor environments. It is important to evaluate algorithms considering these environments, i.e. for unbalanced camera condition, photometric lighting conditions like mutual reflection, shadow, noise, image complexity. We performed evaluation based on natural stereo image pairs from an outdoor scene and an indoor scene in Figure 5. A "Balloon" color stereo image pair with size of 720×480 pels and 24bits/pel is used because it contains difficult lighting conditions with imbalance between left and right images (i.e. left image is darker than right image). Several objects

have different disparities. The "Buggy" stereo image pair of same size and color resolution has more stable lighting conditions between left camera and right camera. However, it has non-texture areas which have similar color and intensity values in the foreground and the background. The non-texture areas easily cause ambiguous matching problems.

The proposed algorithm yields excellent dense disparity maps as shown in Figure 6. The left image is the left-to-right disparity map. Brighter values represent large disparity vectors. The right image is the right-to-left disparity map.

(a) Balloons

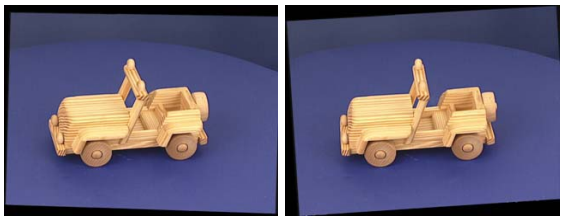

(b) Buggy

Figure 5. Simulation datasets

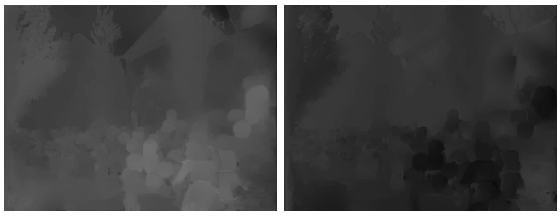

(a) Balloons

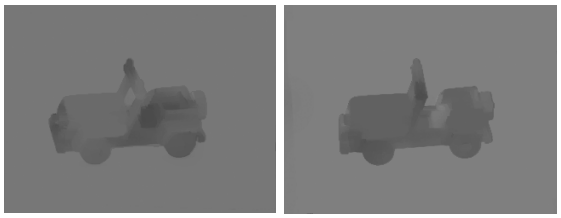

(b) Buggy

Figure 6. Simulation results

While iteration is used to solve the PDE, the dense disparity field is estimated and regularized with anisotropic diffusion. In the nonlinear regularization term, an edge-stopping flux function which uses a combination between the gradient of a Gaussian scale-space and the gradient of a disparity field provides an excellent localization performance of discontinuity and homogeneous condition. In the coarse-to-fine hierarchy, the occlusions of final fine depth fields are diffusively filled using coarse disparity fields. This is an attractive, fully-automatic approach since the method generates a natural complete disparity without an additional occlusion hole filling step. Thus our algorithm avoids usual post-processing to synthesize non-information region of occlusion using interpolation, extrapolation and mirroring.

3.2. Performance comparison

Although the proposed algorithm results shown in Figure 6 suggest a good performance, comparison of large-baseline scenes between the proposed algorithm and some traditional algorithms are important. Large-baseline dense disparity estimation is a challenging task, since it is usually difficult to obtain good correspondences across images. If the baseline is large, epipolar geometry must be calculated before disparity matching.

Large-baseline stereo sequence data sets, "Teddy" and "Kate" in Figure 7 are used for the evaluation. The size of "Teddy" is 450×375 pels and the size of "Kate" is 320×240 pels. Sequence "Teddy" is based on parallel camera geometry while sequence "Kate" is taken from toed-in cameras. The baseline is very large and the image is not rectified. Figure 8 depicts the results of various of traditional methods and the proposed algorithm.

"SSD" is a pixel-based matching algorithm using a sliding window to calculate as error criteria the sum of squared differences. SSD produces large error as shown in Figure 8-(a). A fixed window increases the likelihood of mismatch per pixel. Moreover, very large baseline causes serious matching errors as seen in the "Kate" image. "Graph-cut" requires heavy computation but is the approach is well-known as most reliable global optimization algorithm. Graph-cut handles links-and-cuts of multiple possible values by repeatedly minimizing an energy function involving only binary variables. The algorithm provides stable result for very large baseline, but problems appear with high disparity values as shown in Figure 8-(b). On the contrary, the proposed method

in Figure 8-(c) represents the most reliable and detailed disparity maps. The performance comparison proves the excellent performance of the proposed algorithm.

(a) Teddy

(b) Kate

Figure 7. Large-baseline datasets

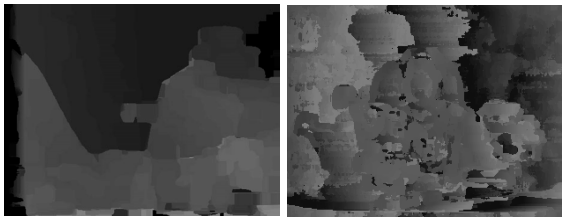

(a) SSD

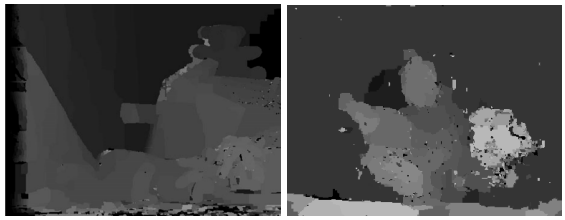

(b) Graph-cut

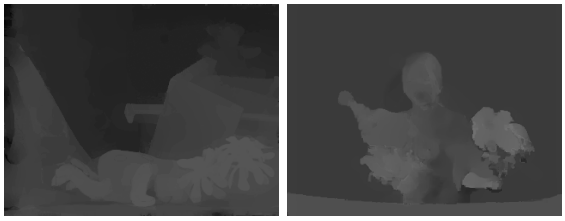

(c) Proposed algorithm

Figure 8. Performance comparison

4. Conclusions

In this paper we proposed a new, reliable dense stereo correspondence method which is called Gaussian scale-space dense disparity estimation with anisotropic disparity diffusion.

We described the algorithm with two steps: (1) Gaussian scale-space disparity initialization and (2) Dense disparity estimation with anisotropic disparity-field diffusion. The algorithm establishes the progressive combination between dense disparity estimation and a regularization method using the anisotropic diffusion on a multi-scale hierarchy generated by Gaussian-filter kernel. The multi-scale approach provides the best trade-off between the detection and localization performance. Moreover, pre-filtered processing solves convergence into local minima in areas of large gradients in PDE. Therefore, our algorithm brings about the excellent localization characteristics of a dense disparity field by only tuning few parameters. We evaluate the performance using an outdoor scene and an indoor scene and achieved excellent results. A comparison with traditional algorithms proves the excellent performance on the large-baseline as well.

5. Acknowledgement

This work was developed within VISNET, European Network of Excellence (*http://www.visnet-noe.org*) funded under the European Commission IST FP6 program.

6. References

[1] L. Robert, O.D. Faugeras, "Curve-Based Stereo: Figural Continuity And Curvature", in *Proceeding of IEEE Computer Society Conference on Computer Vision and Pattern Recognition*, pp. 57-62, 1991.

[2] J. Konrad, Z. D. Lan, "Dense disparity estimation from feature correspondences", in *Proceding of SPIE Stereoscopic Displays and Virtual Reality Systems*, vol. 3957, pp. 90-101, 2000.

[3] L. Di Stefano, M. Marchionni, S. Mattoccia, "A Fast Area-Based Stereo Matching Algorithm", *Image and Vision Computing*, vol. 22, pp. 983-1005, 2004

[4] P. Fua, "Combining Stereo and Monocular Information to Compute Dense Depth Maps that Preserve Discontinuities", in *Proceeding of 12th International Joint Conference on Artificial Intelligence*, 1991.

[5] R. Maas, B. M ter Haar Romeny, M. A. Viergever, "Area-based computation of stereo disparity with model-based window size selection", in *Proceeding of IEEE*

Computer Society Conference on Computer Vision and Pattern Recognition, 1999.
[6] S. Birchfield, C. Tomasi, "Depth Discontinuities by Pixel-to-Pixel Stereo", *International Journal of Computer Vision*, pp. 269-293, 1999.
[7] A. Fusiello, V. Roberto, and E. Trucco, "Efficient stereo with multiple windowing", in *Proceeding of IEEE Computer Society Conference on Computer Vision and Pattern Recognition*, pp. 858-863, 1997.
[8] T. Kanade, M. Okutomi, "A stereo matching algorithm with an adaptive window: theory and experiment", *IEEE Transactions on Pattern Analysis and Machine Intelligence*, vol. 16, pp. 920-932, 1994.
[9] M. Agrawal, L. S. Davis, "Window-based, discontinuity preserving stereo", in *Proceeding of IEEE Computer Society Conference on Computer Vision and Pattern Recognition*, vol. 1, 2004.
[10] Ru-Shang Wang and Yao Wang, "Multiview Video Sequence Analysis, Compression, and Virtual Viewpoint Synthesis", *IEEE Transactions on Circuits and Systems for Video Technology*, vol. 10, pp. 397-410, 2000.
[11] L. Alvarez, J. Sánchez, "3-D Geometry reconstruction using a color image stereo pair and partial differential equations", *Cuadernos del Instituto Universitario de Cienciasy Tecnologas Ciberneticas*, vol. 6, pp. 1-26, 2000.
[12] L. Alvarez, R. Deriche, J. Sánchez, and J. Weickert, "Dense disparity map estimation respecting image derivatives: a PDE and scale-space based approach", *Journal of Visual Communication and Image Representation*, vol. 13, 2002.
[13] C. Strecha, L. Van Gool, "PDES-based multi-view depth estimation", in *Proceeding of 1st International Symposium on 3D Data Processing Visualization and Transmission*, pp. 416-425, 2002.
[14] P. Liatsis, J. Y. Goulermas, "Depth estimation from stereo using a constrained non-linear programming framework", in *Proceeding of 4th European Workshop Image Analysis for Multimedia Interactive Services*, pp. 369-374, 2003.
[15] H. Kim and S. Sohn, "Hierarchical Depth Estimation for Image Synthesis in Mixed Reality", in *Proceeding of SPIE Electronic Imaging*, pp. 544-553, 2003.
[16] R. Deriche "Dense Depth Map Reconstruction: A Minimization and Regularization Approach which Preserves Discontinuities", in *Proceeding of 4th European Conference on Computer Vision*, pp. 439-451, 1996.
[17] P. Perona, J. Malik, "Scale-space and edge detection using anisotropic diffusion", *IEEE Transactions on Pattern Analysis and Machine Intelligence*, pp. 629-639, 1990.
[18] F. Catt´e, P. L. Lions, J. M. Morel, and T. Coll, "Image selective smoothing and edge detection by nonlinear diffusion", *SIAM Journal Numerical Analysis*, vol. 29, pp. 182-193, 1992.
[19] J. Weickert, "Foundations and applications of nonlinear anisotropic diffusion filtering", *Zeitschrift für angewandte Mathematik und Mechanik*, pp. 283-286, 1996.
[20] J. Canny, "Computational approach to edge detection", *IEEE Transaction on Pattern Analysis and Machine Intelligence*, vol 8, pp. 679-698, 1986.
[21] A. P. Witkin, "Scale-space filtering", in *Proceeding of 8th International Joint Conference on Artificial Intelligence*, pp. 1019-1022, 1983.
[22] R. Deriche, "Optimal edge detection using recursive filtering", in *Proceeding of IEEE International Conference on Computer Vision*, pp. 501-505, 1987.
[23] Y. Dufournau, C. Schmid, R. Horaud, "Image matching with scale adjustment", *Computer Vision and Image Understanding*, vol. 93, 2004, page 175-194.
[24] C. Menard, W. G. Kropatsch, "Adaptive Stereo Matching in Correlation Scale-Space", in *Proceedings of the 9th IAPR International Conference on Image Analysis and Processing*, vol. 1, pp. 677-684, 1997.
[25] W. Ma, B. S. Manjunath, "EdgeFlow: a technique for boundary detection and image segmentation", *IEEE Transaction on Image Processing*, pp. 1375-1388, 2000.
[26] M. J. Black, G. Sapiro, D. H. Marimont, D. Heeger, "Robust anisotropic diffusion", *IEEE Transactions on Image Processing*, vol. 7, page 421-432, 1998.
[27] S. K. Weeratunga, C. Kamath, "A comparison of PDES-based non-linear anisotropic diffusion techniques for image denoising", in *Proceeding of SPIE Electronic Imaging, Image Processing: Algorithms and Systems II*, 2003.